DESIGN OF NSLS-II LATTICE WITH COMPLEX BEND REPLACEMENT

M. Song*, Y. Hidaka, B. Kosciuk, T. Shaftan, G. Wang,
Brookhaven National Laboratory, Upton, United States

Abstract

The demands of a higher-brightness photon beam push the electron beam emittance of storage rings toward a diffraction-limited level. The complex bend lattice offers a new approach to achieve low beam emittance. To pave the way for a full lattice upgrade, NSLS-II is planning to replace two existing dipoles with complex bends as a feasibility demonstration. This paper presents the design of the NSLS-II lattice with high-gradient complex bend replacement. Nonlinear beam dynamics are optimized to provide sufficient dynamic and momentum apertures for off-axis injection and reliable operation. In addition, the robustness of the optimized lattice to realistic errors is also evaluated.

INTRODUCTION

In recent decades, beamline users have demanded brighter synchrotron radiation. To meet this need, storage rings have continued to lower the beam emittance in order to increase the photon beam intensity. Since beam emittance ϵ scales as $\epsilon \propto 1/N_d^3$ [1], increasing the number of dipoles N_d in a storage ring is an effective way to reduce emittance. As a result, fourth-generation storage ring light sources around the world use multi-bend achromat (MBA) lattices [2–6]. In these lattices, the number of bending magnets is higher than in the double-bend achromat (DBA) [7] or triple-bend achromat (TBA) [8] used in third-generation light sources. However, if the goal is to push the emittance even closer to the diffraction limit within the same storage ring tunnel, it becomes more difficult to provide enough space for ring elements and insertion devices (IDs). For example, a lattice option for MAX-IV upgrade uses a 19-BA achromat and can reach 16 pm·rad in a 500-meter ring tunnel [9]. This design offers high performance by reducing the emittance by a factor of 20 compared to the current MAX-IV ring. However, the arrangement of the lattice elements leaves very little space for IDs and other ring equipment.

This example adequately illustrates the limit of the MBA approach in its current form. Therefore, it motivates the search for new accelerator technologies and lattice solutions. One method adopted in next-generation storage ring upgrades is the use of complex bend (CB), a new magnet concept first proposed for the NSLS-II upgrade [10]. The CB has gone through several stages of development. The initial concept consisted of a series of short dipole magnets interleaved with strong quadrupoles [11]. It then evolved into a design in which the quadrupoles were shifted transversely to generate dipole fields [12]. More recently, it has advanced to the current design, which uses permanent-magnet dipole-quadrupole combined-function magnets (PMQs), in either Halbach or hybrid type [13, 14]. Using this latest version of the CB, low-emittance storage ring designs have been developed for the NSLS-II upgrade at beam energies of 3 GeV [15] and 4 GeV [16].

To evaluate the potential limitations and technical challenges introduced by the CB lattice, a new installation project has been initiated at NSLS-II to replace the existing two dipoles with CBs, as shown in Fig. 1. This modification will allow beam dynamics with CBs to be studied during regular machine operation. However, it breaks the symmetry of the current NSLS-II lattice [17]. Relevant simulation and experimental studies of a developed asymmetric NSLS-II lattice are reported in [18]. To reduce the impact on normal operation, the modified asymmetric lattice must preserve high injection efficiency and long beam lifetime. In this work, we developed an NSLS-II lattice with two CB replacements and performed a nonlinear beam dynamics optimization of the modified lattice. The results show that the performance degradation caused by the lattice change can be mitigated through further optimization. In addition, we carried out a comprehensive error analysis to demonstrate the robustness of the developed lattice. These studies provide a basis for the smooth installation of CBs and for a future upgrade of the NSLS-II to a CB-based lattice.

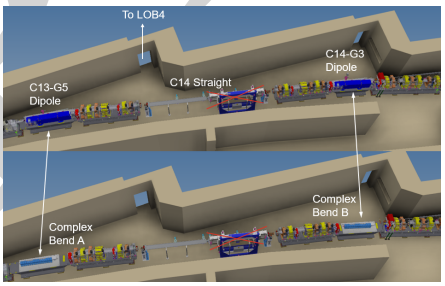

Figure 1: Schematic layout of the dipole replacement with CB magnets in Cells 13 and 14 of the NSLS-II storage ring.

LATTICE WITH COMPLEX BENDS

The NSLS-II storage-ring lattice consists of 30 cells, each based on a DBA structure [17]. The lattice with CB replacements was developed from the NSLS-II operational lattice, specifically the 17-IDs lattice.

To replace a 2.62-meter-long NSLS-II dipole with a bending angle of 6 degrees, a symmetric dipole replacement scheme was used to preserve the overall optics symmetry, with the dipoles on Girder 5 in Cell 13 and Girder 3 in Cell 14 selected for replacement. The CB magnet includes not only focusing PMQ (CB-BQF) and defocusing PMQ (CB-BQD) elements, but also pure dipole (CB-B) elements to provide the required bending angle and to match the floor coordinates. In addition, the CB-BQD and CB-BQF are

* msong1@bnl.gov

placed next to each other with a distance similar to the pole distance considered for the future upgrade of NSLS-II. However, due to the minimum required local physical aperture of 18 mm, both the magnetic field and the gradient are limited. The replacement of the dipoles with CB magnets modifies the local optics. To compensate for these changes, nearby quadrupoles are re-tuned to match the local optics, while keeping their gradients below the limit of 22 T/m and maintaining global parameters, such as tunes and chromaticities, within acceptable ranges. The parameters of the designed CB magnet, determined by coordinate and optics matching, are listed in Table1. According to Table 1, the CB fields and gradients are higher than those of existing dipoles and quadrupoles, and the corresponding pole-tip fields ($\mathbf{B_{max}}$) are comparable to those planned for future upgrade. Here, $\mathbf{B_{max}} = \mathbf{B} + \mathbf{G} \times \mathbf{r}$, where $\mathbf{r}$ is the magnet bore radius, taken here as 12 mm.

Table 1: Complex Bend Parameters

	L [cm]	B [T]	G [T/m]	B_{max} [T]
CB-B	20/30	0.52		
CB-BQD	10	0.66	−53.86	1.31
CB-BQF	10	0.38	60.41	1.11

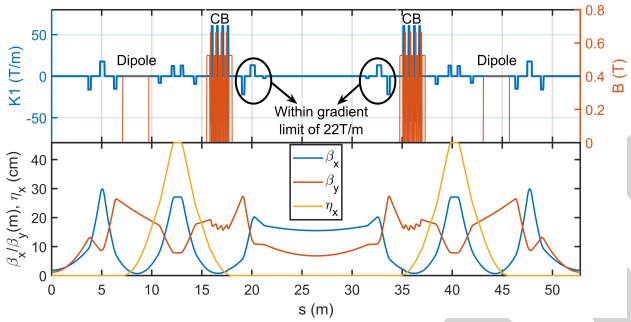

Figure 2: Lattice with CBs and the corresponding Twiss functions in Cells 13 and 14.

Moreover, slight adjustments were made to restore the tunes and chromaticities to their nominal values. Figure 2 shows the developed lattice with CBs and the corresponding Twiss functions in Cells 13 and 14. The beta functions oscillate in the CB region due to the alternating focusing and defocusing elements. It is worth noting that the local emittance contributions have only a minor effect on the total storage ring emittance.

NONLINEAR DYNAMICS OPTIMIZATION

In the developed NSLS-II 17-IDs lattice with CBs, the CBs modify the linear optics and break the lattice symmetry, which degrades the nonlinear beam-dynamics performance, as shown in Fig. 3. Therefore, further optimization is required to recover the performance, in particular, by increasing the dynamic aperture (DA) and momentum aperture (MA) to sufficient levels. The NSLS-II storage ring has six harmonic sextupole families: SL1, SL2, and SL3 in the low-beta straights and SH1, SH3, and SH4 in the high-beta straights. In DA and MA optimization, changes to the sextupole power supplies are kept as small as possible by using three pairs of local power supplies for the sextupoles SH1G6C13B/SH1G2C14A, SH3G6C13B/SH3G2C14A, and SH4G6C13B/SH4G2C14A, which are independent of the shared pentant circuit. These sextupoles are, therefore, grouped into three local knobs and optimized separately. The SH1, SH3, and SH4 sextupoles in the remaining high-beta straights are grouped into three additional knobs. The SL1, SL2, and SL3 sextupoles in all low-beta straights are grouped into another three knobs. As a result, the DA and MA optimization uses a total of nine control knobs. In addition, the strength of each harmonic sextupole is constrained to remain within the current operational limit of 40 T/m^2. The optimization is performed by simultaneously improving both DA and MA. Here, DA and MA are evaluated as the maximum stable area in the transverse x-y plane and the maximum momentum deviation at the injection point, respectively. Following optimization, a solution is selected based on its overall performance in terms of both DA and MA. With optimized sextupole settings, the DA of the 17-IDs lattice with CBs is significantly improved and restored to the nominal level, as shown in Fig. 3.

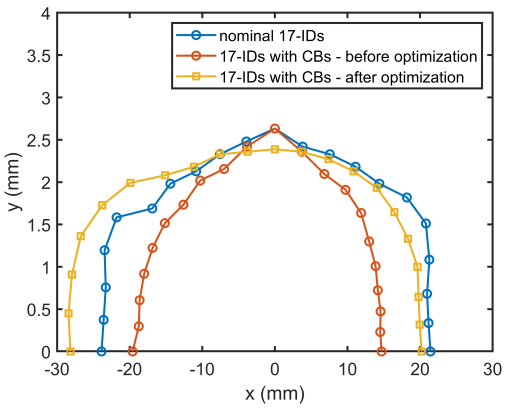

Figure 3: Comparison of the dynamic aperture for the nominal 17-IDs lattice and the 17-IDs lattice with CBs, before and after optimization at the injection point.

In addition to the contour and area of the DA, frequency maps [19] in the x-y and x-δ planes are used to characterize the underlying nonlinear dynamics. Although the DA identifies the region of stable motion, it does not directly reveal the mechanisms that limit stability. Figure 4 compares the frequency maps for the nominal 17-IDs lattice and the optimized 17-IDs lattice with CBs, where the color scale denotes the tune diffusion rate. This comparison provides additional information on the impact of CBs on the nonlinear dynamics.

The frequency map in the x-y plane shows the effects of transverse nonlinearities, coupling, and resonance excitation on particle motion. The frequency map in the x-δ plane provides complementary information on off-momentum dynamics, including chromatic nonlinearities and resonance

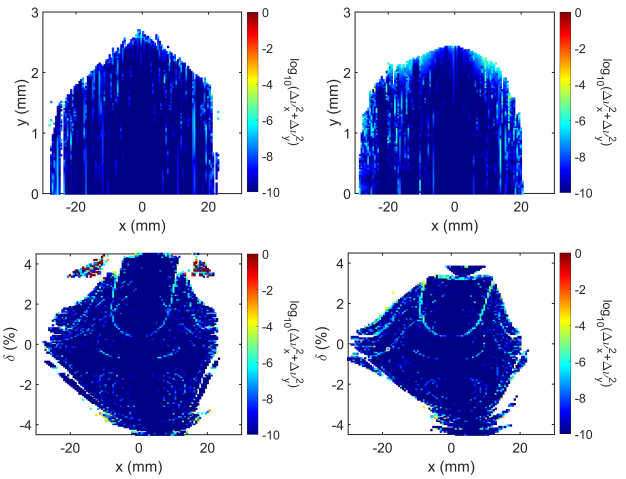

Figure 4: Comparison of the frequency maps for the nominal 17-ID lattice (left column) and the optimized 17-IDs lattice with CBs (right column) in the x-y (upper row) and x-δ (lower row) planes. The color scale denotes the tune diffusion rate.

behavior as a function of momentum deviation. Comparison of the two lattices makes it possible to identify changes in resonance structure and diffusion rate introduced by the CBs. Together, these maps help identify the origin of aperture limitations and provide guidance for nonlinear optimization.

ERROR ANALYSIS

Although the optimized lattice recovers the desired beam dynamics performance in the ideal machine, its robustness must also be evaluated under realistic conditions. In practice, magnet imperfections and alignment errors can perturb both the linear optics and the nonlinear beam dynamics, leading to orbit distortion, beta beat, tune shifts, and a reduction of DA and MA. It is therefore necessary to perform an error analysis to assess the sensitivity of the designed 17-IDs lattice with CBs to such imperfections and to verify that the lattice performance remains acceptable in the presence of realistic machine errors being corrected.

The error model used in this study is summarized in Table 2. The rms values and cutoffs for the BPM, quadrupole, sextupole, and girder offset, roll, and fractional strength errors (FSEs) are taken to be the same as those used for the existing nominal 17-IDs lattice. Separate error specifications are defined for the CB magnets. For the CB magnets, the error model includes not only offset, roll, and FSEs, but also higher-order multipole field errors. The adopted rms values and cutoffs are based on levels achievable with current magnet fabrication and alignment technology. For each random seed, errors are generated according to the rms values listed in Table 2, with the corresponding cutoff applied to each distribution. This error model is used to represent realistic static machine imperfections in the 17-IDs lattice with CBs.

For each random error seed, closed orbit correction is first performed using 360 correctors and 360 beam position monitor (BPM) readings, with 180 correctors and 180 BPMs in each transverse plane. After orbit correction, tunes, beta beat, dispersion, and coupling corrections are carried out using 330 quadrupoles, including 300 normal quadrupoles and 30 skew quadrupoles. These corrections are based on the corresponding response matrices and are solved using the singular value decomposition (SVD) method. The correction procedure is iterated until the residual orbit and optics functions reach acceptable levels. The corrected lattice was subsequently evaluated in terms of the residual orbit, corrected tunes, rms beta beat, dispersion distortion, emittance, DA, and MA. Repeating this procedure for 100 random seeds provides a statistical assessment of the robustness of the 17-IDs lattice with CBs.

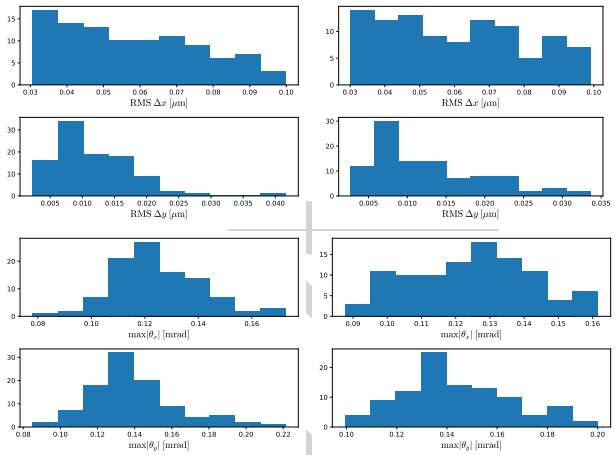

Figure 5: Comparison of the statistical results for 100 random error seeds for the nominal 17-IDs lattice (left column) and the 17-IDs lattice with CBs (right column). The upper row shows the residual orbit after orbit correction, and the lower row shows the maximum required corrector strength for each seed.

Figure 5 shows the statistical comparison of orbit correction results for the nominal 17-IDs lattice and the 17-IDs lattice with CBs over 100 random error seeds. For the 17-IDs lattice with CBs, the histograms in the upper right plot show that the closed orbit is effectively corrected, with the residual orbit remaining below 0.1 μm in x and 0.035 μm in y. Correspondingly, the lower row plots show that the maximum required corrector strengths are comparable to those of the nominal lattice and remain within a practical operating range. These results demonstrate that the use of existing BPMs and correctors is sufficient to correct the orbit of the lattice with CBs.

Figure 6 shows the statistical comparison of optics correction results for the nominal 17-IDs lattice and the 17-IDs lattice with CBs over 100 random error seeds. For the 17-IDs lattice with CBs, the tunes are restored to their nominal values after correction, and the emittance distribution remains nearly unchanged relative to that of the nominal lattice. The rms beta beat is reduced to less than 1% and the rms dispersion is corrected to below 2 mm. These results indicate that the integration of CBs into the lattice does not degrade the

Table 2: Error Parameters and RMS Values

Component	Error Parameter	RMS	Unit	Cutoff (σ)
BPMs	Offset x/y	100	μm	1.0
	Roll	0.2	mrad	1.0
CB-BQD/CB-BQF	Offset x/y	30	μm	1.0
	Roll	0.5	mrad	1.0
	FSE_DIPOLE	0.1%	—	1.0
	FSE_QUADRUPOLE	1%	—	1.0
	K2 (sextupole)	0.7	m^{-3}	1.0
	K3 (octupole)	150	m^{-4}	1.0
CB-B	Offset x/y	30	μm	1.0
	Roll	0.5	mrad	1.0
	FSE_DIPOLE	1×10^{-3}	—	1.0
	K2 (sextupole)	0.7	m^{-3}	1.0
	K3 (octupole)	150	m^{-4}	1.0
QUAD / HIQUAD	Offset x/y	30	μm	1.0
	Roll	0.2	mrad	1.0
	FSE	2.5×10^{-4}	—	1.0
SEXT / HISEXT	Offset x/y	30	μm	1.0
	Roll	0.2	mrad	1.0
	FSE	5×10^{-4}	—	1.0
Girders	Upstream/Downstream offset x/y	100	μm	1.0
	Roll	0.5	mrad	1.0

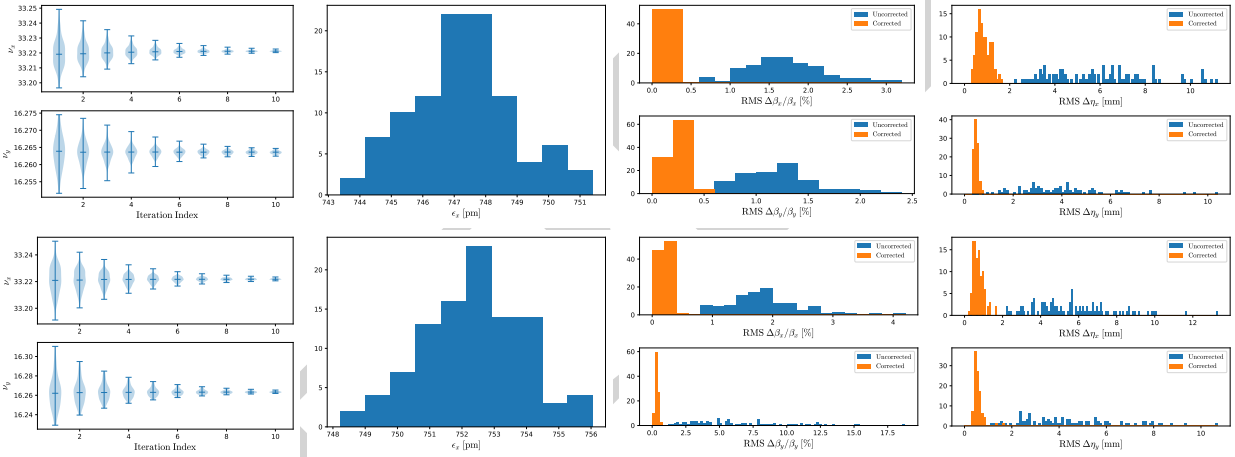

Figure 6: Comparison of the statistical results for 100 random error seeds for the nominal 17-IDs lattice (upper row) and the 17-IDs lattice with CBs (lower row). From left to right, the plots show the corrected tunes, the emittance distribution, the rms beta beat and the rms dispersion before and after optics correction.

optics correction performance in the presence of realistic machine errors.

Following orbit and optics correction, the DA is evaluated for 100 random error seeds and statistically compared for the nominal 17-IDs lattice and the 17-IDs lattice with CBs, as shown in Fig. 7. For both lattices, the DA is reduced compared to the ideal lattice performance because of residual errors after correction. Nevertheless, after correction, the optimized 17-IDs lattice with CBs shows DA performance comparable to that of the nominal lattice. These results indicate that the optimized 17-IDs lattice with CBs remains robust in nonlinear performance in the presence of realistic machine errors.

CONCLUSION

In this work, a 17-IDs lattice with CBs was designed and studied. The CB implementation uses three types of magnetic elements with higher fields and gradients, achieving a pole-tip field comparable to that required for the future NSLS-II upgrade. After further nonlinear optimization, DA and MA were restored to acceptable levels. Then comprehensive statistical error studies were carried out to assess

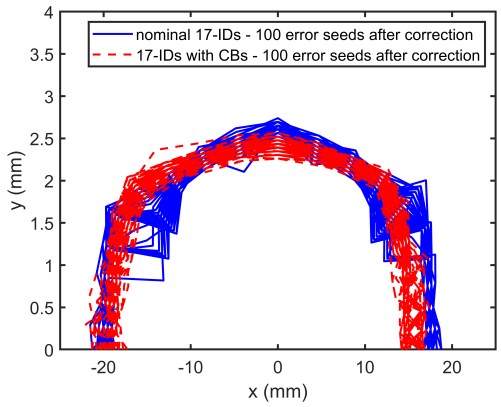

Figure 7: Comparison of the dynamic aperture for 100 random error seeds after orbit and optics correction in the nominal 17-IDs lattice and the 17-IDs lattice with CBs.

the robustness of the designed lattice. The results show that, after orbit and optics correction, the residual orbit, linear optics, and corrected DA are all comparable to those of the nominal 17-IDs lattice. Overall, these results demonstrate that the optimized 17-IDs lattice with CBs is a feasible and robust candidate for practical implementation.

ACKNOWLEDGMENT

This work is supported by the U.S. Department of Energy, Office of Basic Energy Sciences, under Contract No. DE-SC0012704 and Field Work Proposal No. PS043.

REFERENCES

[1] J. B. Murphy, "Synchrotron light source data book", *AIP Conf. Proc.*, vol. 249, no. 2, pp. 1939–2011, 1992. doi:10.1063/1.41969

[2] D. Einfeld, J. Schaper, and M. Plesko, "Design of a Diffraction Limited Light Source (DIFL)", in *Proc. PAC'95*, Dallas, TX, USA, May 1995, paper TPG08, pp. 177–179.

[3] S. C. Leemann, M. Sjöström, and Åke. Andersson, "First optics and beam dynamics studies on the MAX IV 3 GeV storage ring", *Nucl. Instrum. Methods Phys. Res., Sect. A*, vol. 883, pp. 33–47, 2018. doi:10.1016/j.nima.2017.11.072

[4] P. Raimondi *et al.*, "Commissioning of the hybrid multibend achromat lattice at the European Synchrotron Radiation Facility", *Phys. Rev. Accel. Beams*, vol. 24, no. 11, p. 110701, Nov. 2021. doi:10.1103/PhysRevAccelBeams.24.110701

[5] T. E. Fornek, "Advanced Photon Source Upgrade Project Final Design Report", Rep. APSU-2.01-RPT-003, May 2019. doi:10.2172/1543138

[6] C. Steier *et al.*, "Completion of the brightness upgrade of the ALS", *J. Phys. Conf. Ser.*, vol. 493, no. 1, p. 012030, Mar. 2014. doi:10.1088/1742-6596/493/1/012030

[7] R. Chasman, G. K. Green, and E. Rowe, "Preliminary design of a dedicated synchrotron radiation facility", *IEEE Trans. Nucl. Sci.*, vol. 22, no. 3, pp. 1765–1767, 1975. doi:10.1109/TNS.1975.4327987

[8] D. Einfeld and G. Mülhaupt, "Choice of the principal parameters and lattice of bessy, an 800 mev-dedicated light-source", *Nucl. Instrum. Methods*, vol. 172, no. 1, pp. 55–59, 1980. doi:10.1016/0029-554X(80)90607-2

[9] P. F. Tavares, J. Bengtsson, and Å. Andersson, "Future development plans for the MAX IV light source: Pushing further towards higher brightness and coherence", *J. Electron. Spectrosc. Relat. Phenom.*, vol. 224, pp. 8–16, 2018. doi:10.1016/j.elspec.2017.09.010

[10] T. Shaftan, V. Smaluk, and G. Wamg, "Concept of the complex bend", Brookhaven National Lab.(BNL), Upton, NY, United States, Rep., 2018.

[11] G. Wang *et al.*, "Complex bend: strong-focusing magnet for low-emittance synchrotrons", *Phys. Rev. Accel. Beams*, vol. 21, p. 100703, Oct. 2018. doi:10.1103/PhysRevAccelBeams.21.100703

[12] G. Wang *et al.*, "Complex bend. II. A new optics solution", *Phys. Rev. Accel. Beams*, vol. 22, p. 110703, Nov. 2019. doi:10.1103/PhysRevAccelBeams.22.110703

[13] P. N'gotta, G. Le Bec, and J. Chavanne, "Hybrid high gradient permanent magnet quadrupole", *Phys. Rev. Accel. Beams*, vol. 19, no. 12, p. 122401, Dec. 2016. doi:10.1103/PhysRevAccelBeams.19.122401

[14] S. Sharma, "Elements of engineering design of the upgrade lattice", BNL Retreat on Plans for NSLS-II Upgrade, 2023,

[15] M. Song and T. Shaftan, "Design study of a low emittance complex bend achromat lattice", *Phys. Rev. Accel. Beams*, vol. 27, no. 6, p. 061601, Jun. 2024. doi:10.1103/PhysRevAccelBeams.27.061601

[16] M. Song and T. Shaftan, "Design of the low-emittance complex bend lattice", in *Proc. IPAC'24*, Nashville, TN, May 2024, pp. 3233–3236. doi:10.18429/JACoW-IPAC2024-THPC82

[17] K. ROBINSON, "Conceptual design report", Brookhaven National Lab. (BNL), Upton, NY (United States), Rep., Dec. 2006. doi:10.2172/910923

[18] M. Song, G. Wang, and T. Shaftan, "Study of nonlinear beam dynamics of an asymmetric NSLS-II lattice", in *Proc. NA-PAC'25*, Sacramento, CA, USA, Aug. 2025, pp. 1119–1121. doi:10.18429/JACoW-NAPAC2025-THP079

[19] J. Laskar, "Introduction to frequency map analysis", in *Hamiltonian systems with three or more degrees of freedom*, Springer, 1999, pp. 134–150.